Binding of Aminoglycosidic Antibiotics to the Oligonucleotide A-Site Model and 30S Ribosomal Subunit: Poisson−Boltzmann Model, Thermal Denaturation, and Fluorescence Studies

Grace Yang,*[,†] Joanna Trylska,[†,‡] Yitzhak Tor,[†] and J. Andrew McCammon[†,§]

Department of Chemistry and Biochemistry, Howard Hughes Medical Institute, and Department of Pharmacology, University of California−San Diego, 9500 Gilman Drive, La Jolla, California 92093, and Interdisciplinary Centre for Mathematical and Computational Modelling, Warsaw University, Pawinskiego 5A, 02-106 Warsaw, Poland

Received March 14, 2006

The binding of paromomycin and similar antibiotics to the oligonucleotide A-site model and the small (30S) ribosomal subunit has been studied using continuum electrostatics methods. Crystallographic information from complexes of paromomycin, tobramycin, and Geneticin bound to an A-site oligonucleotide, and paromomycin and streptomycin complexed to the 30S subunit was used as a foundation to develop structures of similar antibiotics in the same ribosomal binding site. Relative binding free energies were calculated by combining the electrostatic contribution, which was obtained by solving the Poisson−Boltzmann equation, with a surface-area-dependent apolar term and contributions from conformational changes. These computed results showed good correlation with the experimental data resulting from fluorescence binding assays and thermal denaturation studies, demonstrating the ability of the Poisson−Boltzmann model to provide insight into the electrostatic mechanisms for aminoglycoside binding and direction for designing more effective antibiotics.

Introduction

The aminoacyl-transfer RNA (aa-tRNA) decoding site (A-site), a portion of the 16S ribosomal RNA (rRNA) with a highly conserved sequence within the prokaryotic 30S subunit of the ribosome, is a crucial component of the bacterial translational machinery. It preserves the fidelity of protein translation by overseeing the base-pairing interaction between the stem loops of the anticodon of the aa-tRNA and the codon of the messenger RNA (mRNA). Introduction of aminoglycosidic antibiotics to the A-site can compromise the fidelity of this interaction.

Aminoglycosides are pseudo-oligosaccharides with ammonium groups that bind to specific subdomains of the rRNA.[1] They are categorized by their chemical structure and mechanism of action. Most aminoglycosides that bind in the decoding domain of the 30S subunit consist of a 2-deoxystreptamine (2-DOS) ring with amino sugar ring substitutions at the 4 and 5 positions and 4 and 6 positions.[2] The 2-DOS ring, designated ring II, and ring I, its 4-position substitution, form the neamine moiety. Positions 5 and 6 are the attachment points for ancillary rings (Figures 1 and 2).

The deleterious effects of aminoglycosides on bacterial protein synthesis were first recognized in 1965,[3] even though the exact aminoglycoside binding site, the decoding site, was not discovered until 1987.[4] Recent studies have helped to elucidate the mechanism by which the aminoglycoside interferes with translation.[5−9] According to the primary hypothetical mechanism, during the decoding stage, aminoglycosides induce and stabilize a conformation of the A-site very similar to the native conformation caused by cognate tRNA−mRNA interactions.[7,10−12] Crystal structures of the 30S component of the ribosome have shown that the aminoglycosides' mechanism of action interferes with the proper base-pairing of the tRNA anticodon to the mRNA codon at the ribosomal decoding site (Figure 3).[8,13−17] Upon binding of tRNA, the rRNA changes from the "off" form

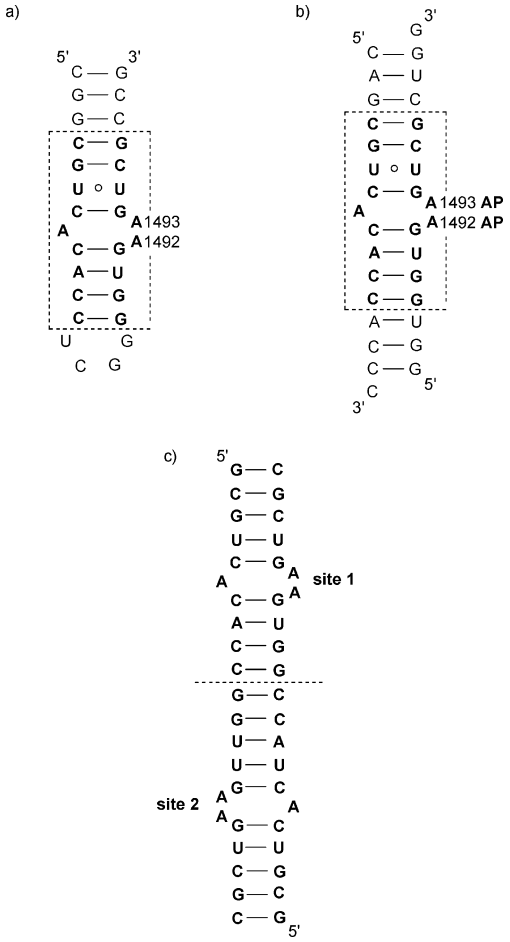

Figure 1. Various A-site oligonucleotides used for (a) thermal denaturation studies, (b) fluorescence studies, and (c) Westhof's crystal structures.

* To whom correspondence should be addressed. Phone: (858) 646-3100, extension 3803. Fax: (858) 795-5285. E-mail: gyang@burnham.org.
† Department of Chemistry and Biochemistry, University of California−San Diego.
‡ Warsaw University.
§ Howard Hughes Medical Institute and Department of Pharmacology, University of California−San Diego.

10.1021/jm060288o CCC: $33.50
Published on Web 08/08/2006

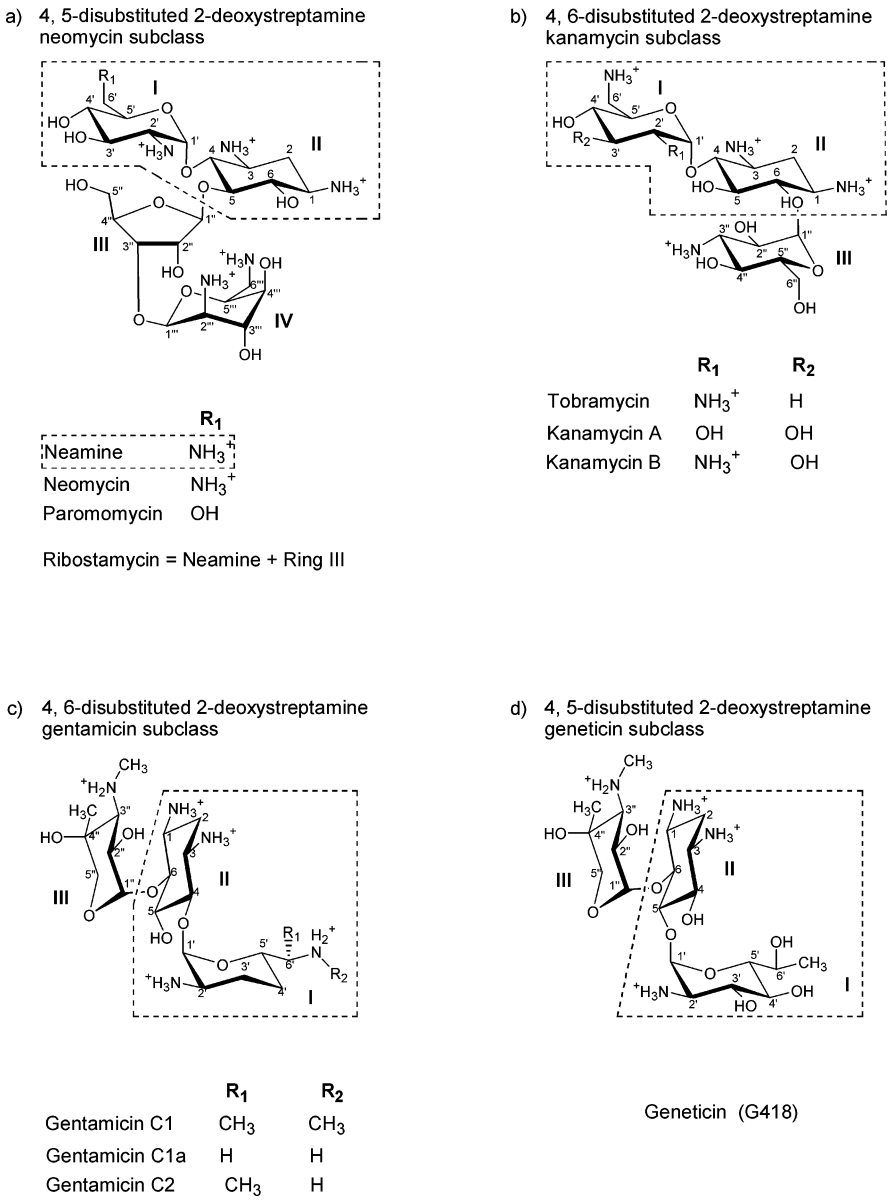

Figure 2. Studied aminoglycosides in their fully protonated states.

to the "on" form by flipping out two adenines (A1492 and A1493) from the shallow groove of the A-site, thus signaling for the advance of translation.[18,19] The conformational change is necessary for A1492 and A1493 to interact with the first two of the three base pairs of the cognate codon−anticodon complex.[19] Aminoglycosides compromise the fidelity of translation by binding to the A-site and stabilizing residues A1492 and A1493 into a conformation that increases the association rate and decreases the dissociation rate of the tRNA anticodon, thus inhibiting translocation and promoting the interaction between noncognate mRNA−tRNA complexes.[18] The binding of the aminoglycoside to the A-site reduces the energetic cost of the ribosomal domain closure required to differentiate between the cognate and noncognate tRNAs.[19]

To facilitate the investigation of this binding mechanism, RNA oligonucleotides containing the minimal bacterial ribosomal A-site have been developed. It has been shown that A-site-containing RNA oligonucleotides bind to aminoglycosides in a manner similar to that of the full ribosome.[20] The Puglisi group developed a 27-mer hairpin oligonucleotide to mimic the A-site region of *E. coli* 16S rRNA and showed that the protection afforded by the aminoglycoside to the oligonucleotide hairpin was almost identical to the protection pattern of the 30S subunit by way of methylation by dimethyl sulfate (DMS) (Figure 1a).[21−23] The Puglisi group also conducted NMR studies on the 27-mer oligonucleotide complexed to paromomycin and gentamicin C1a (Figure 2).[6,23,24] They observed that both paromomycin and gentamicin C1a bind to the major groove of the hairpin in a 1:1 ratio, displacing A1492 and A1493 and creating a network of hydrogen bonds with the RNA.

After the work accomplished by the Puglisi group, the Hermann group was able to investigate the binding between paromomycin and tobramycin to an A-site oligonucleotide modified with a 2-aminopurine (2AP) at the adenine at position 1492 or 1493 (Figure 1b).[16] The fluorescence of 2AP is sensitive to the structural environment because the fluorescence increases with unstacking and exposure to solvent and decreases as it stacks with other bases.[25] The modified RNA oligonucleotides were crystallized and their structures solved to certify that the incorporation of 2AP did not perturb the structure of the decoding site.[16] The fluorescence of 2AP1492 intensifies upon binding of the aminoglycoside because of increased exposure of 2AP1492 to solvent. The inverse occurs with 2AP1493 because stacking to A1492 increases as more aminoglycosides

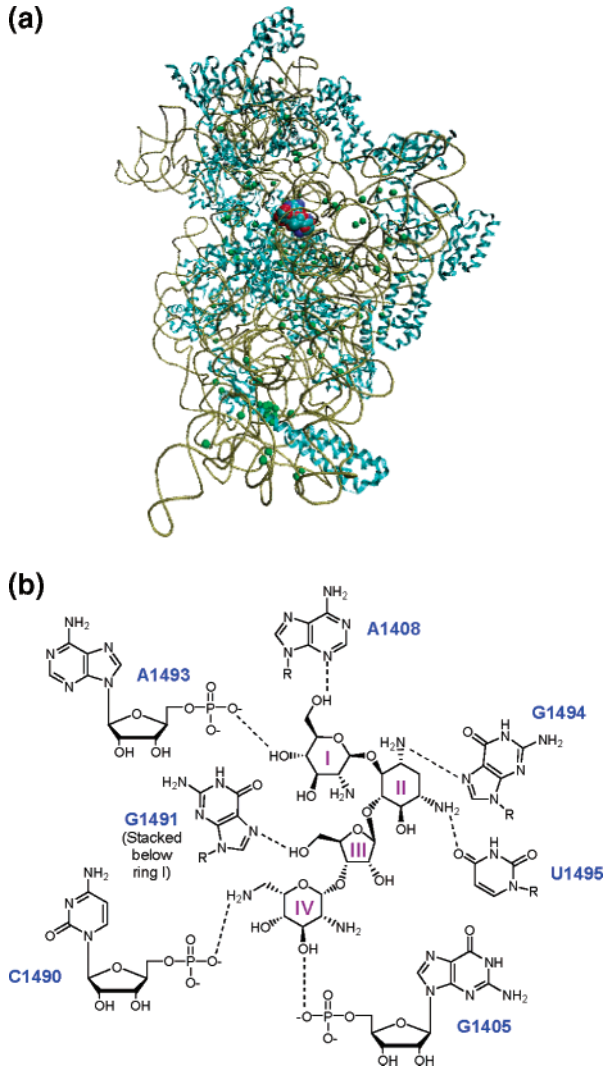

Figure 3. Paromomycin's interaction with A-site of 30S subunit. (a) Paromomycin binding site in the 30S subunit (rRNA is shown in gray, protein chains in cyan, explicit ions in green, and antibiotic as van der Waals spheres). (b) Specific interactions between paromomycin and residues of the 30S subunit.[8]

bind to the decoding region. These 2AP-modified oligonucleotides are useful tools in determining the behavior of the adenines in the A-site upon binding of various aminoglycosides.

The Westhof group was able to obtain the crystal structures of an oligonucleotide containing two A-sites bound to paromomycin, tobramycin, and Geneticin (Figure 1c).[26−28] The details afforded by these crystal structures indicate that the universally conserved 2-DOS ring (ring II) forms similar hydrogen bonds to the shifted U1406−U1495 pair in both the 4,5-substituted and 4,6-substituted aminoglycosides, but the locations of water molecules in the binding site are different.[14] The amino sugar at the 4-position of 2-DOS ring (ring I) of the aminoglycoside stacks against a guanine residue (G1491) and forms two hydrogen bonds to A1408, creating a pseudo-base-pair that is conserved throughout prokaryotes.[11] The remaining rings that are connected to the 2-DOS ring via position 5 or 6 create contacts to different parts of the A-site. Ring III of tobramycin hydrogen-bonds to O6 and N7 of G1405. On the whole, the number of hydrogen bonds created between the RNA and the aminoglycoside in each crystal structure is approximately 25, and regardless of the substitution on the 2-DOS ring, one-third of those hydrogen bonds are water-mediated.[26−28]

A complete understanding of the interactions between the rRNA and the aminoglycosides requires investigation of the thermodynamics involved in the molecular forces controlling the binding interactions. Pilch's group has conducted thermal denaturation and isothermal calorimetry studies on the system of the A-site 27-mer oligonucleotide moiety and neomycin-class aminoglycosides (Figure 1a).[29,30] The group's work demonstrated a few important characteristics of this system. Although the binding of aminoglycosides increases the stability of the RNA, the increase of pH and/or Na^+ causes this stability to decrease. As with the stability afforded by the binding of aminoglycosides to RNA, the observed binding affinities of the aminoglycosides to the RNA decrease with increasing pH and/or Na^+ concentration. Further supporting the dependency of binding energetics to the pH and ionic environment are Pilch's isothermal titration calorimetry (ITC) studies performed as a function of buffer concentration. These indicated that aminoglycoside binding to the RNA is linked to the uptake of protons, and the enthalpies associated with the RNA−aminoglycoside binding become more exothermic with increasing pH, which is in agreement with the binding-dependent protonation of one or more of the aminoglycosidic amino groups.

The binding data and information from previously published studies demonstrate the highly electrostatic nature of the RNA−aminoglycoside binding interaction.[31,32] The aminoglycosidic antibiotics with the greatest affinity for the negatively charged RNA have five or six amino groups that are positively charged at physiological pH. Thus, to understand the inhibition of translation by aminoglycosides, the electrostatic component must be investigated. Because rigorous simulations on the atomic level are currently not feasible for the many antibiotic−30S subunit complexes, we applied continuum electrostatic methods that have been widely used to study the electrostatic properties of biomolecules.[33−35] To look into the energetics of antibiotic binding to the A-site and the 30S subunit, we utilized published crystal structures and modified them to study the electrostatic and nonpolar contributions to the free energy of binding via an algorithm that solves the Poisson−Boltzmann equation (PBE) in continuum solvent and by calculating the amount of solvent-accessible surface area (SASA) buried upon binding. The information obtained from the crystal structures of ribosomal complexes was used to computationally investigate the energetics involved with the binding of antibiotics for which crystal structures do not exist. Although published experimental dissociation constants do exist for most aminoglycosides, they cannot be rigorously compared to one another because they were obtained under different experimental conditions.[36−40] Fluorescence binding and thermal denaturation studies were therefore conducted to obtain a hierarchical affinity under the same conditions, thus yielding values that are comparable and able to validate the computational results.

Materials and Methods

Binding Free Energy Calculations and Fitting of Parameters to Experimental ΔG_{bind}. To calculate the binding free energy, we used the following formula:

$$\Delta G_{calc} = \Delta G_{np} + \Delta G_{elec} + \Delta G_{strain} - T\Delta S_{conf} - T\Delta S_{Tr+Rot} \qquad (1)$$

where ΔG_{elec} and ΔG_{np} are the electrostatic and nonpolar contributions to the binding free energy, $T\Delta S_{Tr+Rot}$ describes the loss of entropy due to a decrease in the number of translational and rotational degrees of freedom, and $T\Delta S_{conf}$ accounts for the reduction in entropy due to the loss of backbone and side chain torsional freedom upon complexation.[41] For the computational values to be fitted to this equation, the terms were interpreted as the following:

ΔG_{calc} is the calculated binding free energy associated with the binding event; ΔG_{np} is the contribution from nonpolar interactions and is proportional to ΔSASA with the microscopic surface tension (γ) as the proportionality coefficient; ΔG_{elec} is the electrostatic component of the binding free energy; ΔG_{strain} represents all other strain and reorganizational change in energy in the system upon ligand binding; $-T\Delta S_{conf}$ represents the entropy loss associated with each ring of the aminoglycoside; $-T\Delta S_{Tr+Rot}$ is equivalent to the translational and rotational entropy loss per ligand estimated on the basis of previously published work.[29] ΔG_{elec} is calculated as the difference between the electrostatic energy for the complex and associating molecules represented on a similar grid and with the same grid spacing to eliminate the grid-based errors. We have previously shown that this approach gives similar results as decomposing ΔG_{elec} into the solvation and Coulombic contributions.[42] The parameters of the above equation that were subject to fitting to experimental data were γ, the amount of conformational entropy loss per aminoglycosidic ring or per entire aminoglycoside, and ΔG_{strain}.

Preparation of the System for ΔG_{elec} Calculations. The electrostatic calculations were based on Poisson−Boltzmann theory. For many years, this theory has been successfully applied to biological molecules, and the details of its implementation and application to such systems may be found in the following papers.[4,33−35] In this model, a molecule is represented as a low dielectric medium containing fixed charges and the solvent is represented as a continuous medium of a high dielectric constant, which contains mobile counterions that screen the fixed charges according to the Debye−Hückel model. The calculations were done using the full nonlinearized Poisson−Boltzmann equation (NPBE) and its linear approximation, i.e., the linearized Poisson−Boltzmann equation (LPBE). Adaptive Poisson−Boltzmann Solver (APBS)[43] was utilized to calculate the electrostatic contributions to the binding free energy (ΔG_{elec}) for the aminoglycoside based antibiotics to the A-site oligonucleotide and the 30S subunit. Fully atomic simulations with explicit solvent are currently not feasible for the many antibiotic−30S subunit complexes. Westhof's construct was used to validate the implicit solvent PB methodology prior to application on the 30S system. Both systems were treated with implicit solvation models to bypass the 30S system's large size and to subject Westhof's construct to the same computational conditions. The electrostatic calculations were performed on an automatically configured sequential focusing multigrid. The continuum solvent dielectric constant (ϵ) was set at 78.5 and for the solute interior at either 4 or 12 to account both for the electronic polarizability and for structural reorganization. Tests with ϵ equal to 2 were also performed, but because of the high charge of the system, they resulted in ΔG_{elec} values that were too large. The initial boundary condition for the LPBE and NPBE calculations was set as a single Debye−Hückel sphere, and later the focusing method was used.[44] The calculations were done in an ionic strength of 150 mM of monovalent ions with an ion exclusion radius of 2 Å at a pH of 7.0.

Charges and radii of the atoms were assigned to the macromolecule according to AMBER8 force field parameters.[45] In case of the 30S subunit, the terminal protein residues were kept charged, as well as Asp, Glu, Arg, and Lys. The net charge of His (pK_a = 6.0) and all other amino acids was set to zero. The few necessary modifications to the aminoglycosides consisted of simple exchanges of similar sized atoms (e.g., N → O); so in order to maintain the configuration as given in the crystal structure, the positions of those heavy atoms were not optimized. Hydrogens were added to the crystal structures, and the aminoglycosides were modified within the Insight II 2000 software package.[46] The positions of hydrogens were energy-minimized in the presence of the 30S subunit or the Westhof construct with the SANDER program and with 1000 steps of the steepest descent method. The shape of the solute was defined by its molecular surface using a probe sphere radius of 1.4 Å. The partial charges for the antibiotics were assigned with the bcc option in the ANTECHAMBER application.[47] The aminoglycosides were determined to be fully protonated, as extrapolated from the analysis of the paromomycin protonation state by Barbieri et al.[30] The sensitivity of the calculations to the force field used was checked by performing a test set of calculations also with Charmm22 parameters and with hydrogen atoms assigned with the HBUILD utility of CHARMM.[48] For example, for ΔG_{elec} for paromomycin binding to the 30S subunit with a net charge of $+4e$ and for dielectric constants of 4 and 12, the Amber8 force field gives less favorable electrostatic contribution than Charmm22 by 12 and 16kJ/mol, respectively. For paromomycin with a net charge of +5e this difference is the opposite; ΔG_{elec} obtained with Amber8 force field is 62 and 29 kJ/mol more favorable than the one obtained with Charmm22 parameters, for $\epsilon = 4$ and $\epsilon = 12$, respectively. The effect of protonation of one site in paromomycin is twice bigger with the Amber8 force field, suggesting that ΔG_{elec} calculated on the basis of Amber8 parameters is more sensitive to the change of charged groups in the ligand. Although the absolute values of the ΔG_{elec} differed, the sign of this contribution and the relative order of binding were similar with both sets. We chose to perform simulations with Amber8 force field because of the bigger sensitivity to change in protonation.

The difference in SASA for the system was calculated by subtracting the SASA of the unbound macromolecule and the aminoglycoside from the SASA of the complex. The acc utility of APBS was used for calculating SASA of the various components.

Westhof A-Site Construct. The coordinates used for the decoding site calculations were obtained from the Protein Data Bank[49] entry codes 1J7T, 1LC4, and 1MWL with resolutions of 2.5, 2.54, and 2.4 Å and bound to paromomycin, tobramycin, and Geneticin (G418), respectively.[26−28] All three structures have the identical RNA comprising two A-sites engineered by Westhof et al. as the macromolecule. According to our calculations, binding of aminoglycosides to the two A-sites are energetically similar; thus, it appears that the two binding events may be noncooperative. The aminoglycosides analyzed within Westhof's A-site construct in this study are neomycin, paromomycin, ribostamycin, neamine, tobramycin, kanamycin A, kanamycin B, G418, gentamicin C1, gentamicin C1a, and gentamicin C2 (Figure 2). The PB calculations for RNA−aminoglycoside complexes were obtained to grid resolutions of 0.3 Å. The calculations were performed using both the LPBE and the NPBE.

There were no Mg^{2+} or Zn^{2+} ions in the crystal structures for the Westhof construct, but individual explicit water molecules were identified. However, only the waters within a 5 Å radius sphere around the antibiotic were treated as explicit water molecules (all other solvent was treated as bulk water). These waters are more likely to be organized, and on the basis of the crystal structure of the complex, they participate in the actual binding event because of their proximity to the binding site. The same explicit waters, which were assigned the partial charges and radii as of AMBER8 force field, were present in the calculations for both the complex and the free A-site construct and kept in the same positions to avoid the dependence of calculations upon the choice of the grid. Such explicit treatment of waters participating in the hydrogen bond formation and mediating the binding ensures proper treatment of the water-mediated hydrogen bonds and avoids the possibility that in these regions implicit solvent would not be accounted for and they would be treated with a low dielectric, that of the solute. The presence of these water molecules makes the electrostatic contribution to binding energy more favorable, which is most likely due to the water molecules' role in stabilizing the binding through hydrogen bonds. The implicit−explicit treatment of the water in the system resulted in calculated free binding energies that were more congruent with the experimental data than the calculations performed on a system where all the water is treated as a dielectric continuum.

30S Subunit. Coordinates for the 30S subunit were obtained from the crystal structure of the Thermus thermophilus 30S subunit bound to paromomycin with resolutions of 3.3 Å (PDB entry code 1FJG).[8,11] The 30S structure occupies a box of roughly 190 × 200 × 150 $Å^3$. The number of IBM Data Star SDSC processors used for the APBS calculations was 384, which resulted in the grid

spacing dimensions for the LPBE-based calculations of 0.2 Å. Automatically configured parallel focusing multigrid calculations were performed. The 1FJG structure was used to investigate the 30S subunit complexed to neomycin, paromomycin, ribostamycin, and neamine because of its versatility. Since it has streptomycin and spectinomycin bound to the 30S subunit as well, this structure could be used to further investigate other aminoglycoside families.

The Mg^{2+} and the Zn^{2+} ions in the 30S subunit systems were kept in their original positions, as dictated by the crystal structure. The dielectric and ion-accessiblity coefficients were smoothed by a simple harmonic averaging to somewhat reduce the sensitivity to the grid setup. Although APBS calculations were possible for the A-site with both the LPBE and NPBE, the 30S calculations using NPBE did not converge to a reasonable resolution because of the high net charge of the system ($-1052e$) and large number of atoms (88 632 atoms) because these calculations resulted in potentials that were too large for the double-floating point precision of the computer. However, earlier studies have shown that the LPBE is a good enough approximation while studying the order of binding of aminoglycosides,[50] 30S subunit,[51] and other systems.[52]

Aminoglycosides. All aminoglycosides, with the exception of neamine, were purchased as sulfate salts from Sigma (neomycin, paromomycin, ribostamycin, tobramycin, and kanamycin B), Calbiochem (kanamycin A and G418, Geneticin), or Gibco (gentamicin C). The neamine was prepared by refluxing neomycin in methanol and hydrochloric acid.[53] Tris[tris(hydroxymethyl)aminomethane], HEPES [4-(2-hydroxyethyl)-1-piperazineethanesulfonic acid] buffers, sodium cacodylate, and all other inorganic salts were purchased from Fisher (enzyme grade). Amberlite CG-50 type II resin was purchased from Sigma.

All aminoglycosides were purified and isolated as the free base form via ion exchange chromatography.[54] The resin used was Amberlite CG-50 (type II, NH_4^+ form). A column with the approximate dimensions of 2 cm × 20 cm was equilibrated with about 500 mL of water. It was then loaded with 5 mL of a ~50 mg/mL solution of aqueous aminoglycoside sulfate. The column was washed with 500 mL of 0.1 M NH_4OH. The aminoglycoside was the eluted with a 600 mL linear gradient from 0.1 to 1 M NH_4-OH. Ninhydrin staining on TLC plates was used to identify the fractions containing aminoglycoside. The desired fractions were collected, concentrated via rotary evaporation, then washed with 200 mL of water, concentrated again, and lyophilized to dryness. The identities of the aminoglycosides were confirmed by mass spectral analysis. All of the aminoglycosides, with the exception of G418 and gentamicin, were purified and supplied by Dr. Ken Blount.

The separation of neomycin sulfate (B and C mixtures) was performed by Dr. Ken Blount. The neomycin mixture was protected as the *tert*-butoxycarbonyl derivative,[55] at which point the B and C isomers could be separated by silica gel flash column chromatography. Neomycin B eluted at 5.75% methanol in dichloromethane, while the C isomer eluted at 6.5% methanol in dichloromethane. The individual neomycins were deprotected in trifluoroacetic acid and then purified via ion-exchange chromatography, as with the other aminoglycosides, resulting in their free base form. Only neomycin B was used in the thermal denaturation studies and will be referred to as neomycin.

RNA Oligonucleotides. All A-site oligonucleotides were purchased from Dharmacon RNA Technologies (Lafayette, CO), deprotected as directed by the manufacturer's protocol, and lyophilized. The deprotected oligonucleotides were resuspended in water and purified using 20% denaturing PAGE (polyacrylamide gel electrophoresis). The desired bands were excised from the gel and were eluted overnight into a buffer comprising 50 mM HEPES, pH 7.5, and 1 M NaCl, followed by ethanol precipitation. The RNA precipitate was subjected to a 70% ethanol/water wash, dried, and resuspended in water. The concentration of the oligonucleotide was quantitated via UV absorption spectroscopy using an extinction coefficient at 260 nm of 248 370 ± 940 at 85 °C.[17] The identity of the oligonucleotide was determined by MALDI-TOF mass spectrometry. The A-site stock solutions for the fluorescence binding experiments were prepared with an oligonuclueotide concentration of 15 μM in HEPES binding buffer (100 mM HEPES, 0.5 mM EDTA, 750 mM ionic strength, pH 7.5). For the thermal denaturation studies, the RNA stock solutions had an oligonucleotide concentration of 130 mM in cacodylate buffer (0.2 M sodium cacodylate, 2 mM EDTA, 3 M ionic strength, pH 7.0). The oligonucleotides were hybridized by heating the solution at 65 °C and then slowly cooled to room temperature over a period of 20 min.

Fluorescence Binding Assay. A Perkin-Elmer LS50B fluorimeter was used for all fluorescence measurements for the binding assay. The excitation slit width was 10 nm, and the emission slit width was 20 nm. The samples were excited at 310 nm, recorded three times at a scan rate of 300 nm/min over a range between 320 and 420 nm, and then averaged into a singe composite spectrum. The buffer required for the assay samples is a 20 mM HEPES, 0.5 mM EDTA, pH 7.5, with an ionic strength of 150 mM.

For each experiment, a fluorescence spectrum of a 148 μL solution of buffer without RNA or aminoglycoside was taken as the baseline. Only Raman scattering was observed in the spectral blank and subtracted from all the following spectra in the individual experiment. After the baseline spectrum was recorded, 2 μL of a 15 μM solution of the refolded 2-aminopurine (2AP) substituted oligonucleotide was added (final concentration of 200 nM), the solution was mixed, and a spectrum was recorded. The 1 μL aliquots of aqueous aminoglycoside solution (increasing concentrations from 0.85 to 50 mM, with the exception of paromomycin which had concentrations ranging from 80 nM to 5 mM) were added, and a spectrum was recoded with each added aliquot until the emission from the 2-aminopurine reached saturation. The emission maximum of 370 nm varied less than 1.5 nm over the range of all the aminoglycosides.

The binding isotherms were indicative of a monophasic binding event; thus, the variations in fluorescence can be attributed to a two-state equilibrium model:

$$\text{A-site}_{\text{unbound}} \overset{\text{AG}}{\rightleftharpoons} \text{A-site}_{\text{bound}}\cdot\text{AG}$$

$$[\text{A-site}_{\text{bound}}] = K_a[\text{A-site}_{\text{unbound}}][\text{AG}]$$

The initial fluorescence (I_{unbound}) of the 2AP derivatized A-site in the absence of aminoglycoside ($\text{A-site}_{\text{unbound}}$) is normalized to 1. As the aminoglycoside is introduced to the A-site, the A-site forms a complex with the aminoglycoside ($\text{A-site}_{\text{bound}}\cdot\text{AG}$) and yields a relative fluorescence intensity (I_{bound}). The observed fluorescence can be expressed as the following equation:

$$I_{\text{obs}} = \frac{I_{\text{unbound}}[\text{A-site}_{\text{unbound}}] + I_{\text{bound}}[\text{A-site}_{\text{bound}}]}{[\text{A-site}_{\text{bound}}] + [\text{A-site}_{\text{unbound}}]} = \frac{I_{\text{unbound}} + I_{\text{unbound}}[\text{AG}]/K_d}{1 + [\text{AG}]/K_d} \quad (2)$$

The concentration of the A-site·AG complex in this experiment is much less than the aminoglycoside concentration because of [A-site] being much less than K_d. Thus, the assumption can be made that the concentration of free aminoglycoside, [AG], is equal to the total aminoglycoside concentration. KaleidaGraph was used to perform a least-squares fit to the experimental data using eq 2.

Thermal Denaturation Assay. A Beckman DU series 600 version T spectrophotometer equipped with a thermoelectrically controlled cell holder was used for all thermal denaturation experiments. All samples were measured in cells with a 1 cm path length. The absorbance intensity of wavelength 274 nm was measured over a temperature range 30−100 °C with a 10 s averaging time. The temperature of the samples was raised in 0.5 °C increments and equilibrated for 1 min at each temperature setting. All melting temperatures were obtained via first-derivative calculations. The concentration of RNA in these melting experiment samples was 1 μM in strand, and the ratio of RNA to aminoglycoside is 1:1. The thermal denaturation studies were conducted in

a buffer solution containing 10 mM sodium cacodylate, 0.1 mM EDTA, and enough NaCl to attain an ionic strength of 100 mM and HCl to adjust the pH to 6.0. The pH and the ionic strength of the buffer were determined by previously published thermal denaturation studies.[29] The concentration of the oligonucleotide was 1 μM. The RNA to antibiotic ratio was 1:1.

By use of the following two equations,

$$\Delta H_{VH} = (2 + 2n)RT_m^2\left(\frac{\partial \alpha}{\partial T}\right)_{T=T_m} \quad (3)$$

$$-RT \ln K_T = \Delta H^\circ\left(1 - \frac{T}{T_m}\right) = \Delta G, \quad \text{where } \Delta H^\circ \equiv \Delta H_{VH} \quad (4)$$

the melting temperature of the given aminoglycoside/A-site complex can be used to determine the van't Hoff enthalpy of association for the aminoglycoside/A-site complex (eq 3), which then in turn can be used to calculate the melting transition free energy of each aminoglycoside/A-site complex (eq 4). The aminoglycosides were determined and ranked in their ability to stabilize the A-site oligonucleotide.

These transition free energies were compared to binding free energies obtained from the fluorescence binding data.

Results and Discussion

Although binding constants and binding free energies for various aminoglycosides have been previously published,[36−40] there is a need to obtain reliable relative binding affinities using the same experimental conditions and techniques for each RNA ligand. The differences in previously reported experimental conditions can include the ionic strength, pH, and type of buffer, and differences in instrumentation, as in calibration, accuracy, and method of detection, can significantly affect the outcome of the experiments. The aminoglycoside−RNA system is very susceptible to the differences stated above because the binding is electrostatically driven.[29,31] To acquire a relative order of binding affinity of a group of aminoglycosides, all of them must be subjected to the identical scenarios. Fluorescence binding assays and thermal denaturation studies were conducted in an attempt to obtain a relative order of binding affinity of the following aminoglycosides: neomycin B, paromomycin, ribostamycin, neamine, tobramycin, kanamycin A, kanamycin B, gentamicin C, and G418 (also known as Geneticin).

Fluorescence Binding Assay. The fluorescence experiments were conducted with Hermann's 2AP1492 and 2AP1493 constructs. The 2AP1492 construct resulted in reproducible fluorescence data for the neomycin and gentamicin family of aminoglycosides but not for those of the tobramycin class. The fluorescence data for tobramycin was indicative of a population of A-site/tobramycin complex in flux instead of the expected steady increase of A-site/aminoglycoside population as the concentration of aminoglycoside was increased. The assay was repeated on the tobramycin family of aminoglycosides with the 2AP1493 construct, but the results were just as inconsistent and unreliable as the ones from 2AP1492. This erratic behavior of the tobramycin class of aminoglycosides was not a surprise because the values obtained by Shandrick et al. for the 2AP1493 construct resulted in a 20% margin of error on either side of the mean with their EC_{50} value for tobramycin.[16] A possible explanation for the unpredictable behavior of tobramycin compared to paromomycin may be its inability to position itself and form as many stable interactions as paromomycin in the A-site binding pocket because of its larger size, therefore resulting in erratic fluorescence data.[36] The assay was abandoned for the tobramycin family.

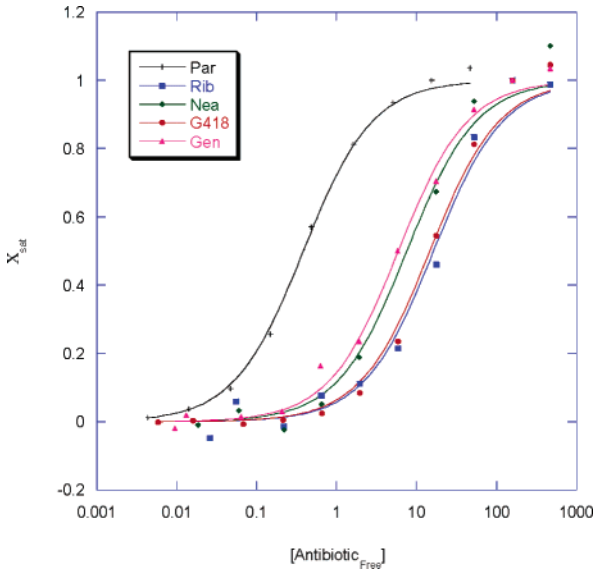

Figure 4. Plot of fractional saturation of the A-site oligonucleotide versus the concentration of free antibiotic.

The concentrations used for the aminoglycosides were identical, with the exception of paromomycin. As a result of paromomycin's high binding affinity, the concentrations used had to be 10-fold lower than the concentrations for the rest of the antibiotics. Neomycin was not used in the fluorescence assay because of its proclivity to cause RNA aggregation in solution. There were three trials for each aminoglycoside, and the mean values of the three trials were obtained, along with their standard deviation. The standard deviation associated with each aminoglycoside is less than one-tenth the mean value, which is indicative of a tight distribution of data points.

The fraction of complexed A-site oligonucleotide was plotted against the concentration of free aminoglycoside, resulting in binding isotherms for paromomycin, ribostamycin, neamine, G418, and gentamicin C (Figure 4). The fluorescence intensified with the increase in aminoglycoside−RNA complex because the 2AP1492 was flipped out of the bulge and exposed to solution upon binding. The relative order of affinity can be deduced visually by the sequence of the isotherms. Paromomycin reached 50% saturation at the lowest concentration of free ligand, as shown by its left-most position on the graph. It is followed by gentamicin C, neamine, G418, and lastly ribostamycin. The fluorescence data were subjected to a least-squares fit to eq 2 to obtain K_d values (shown in Table 1). Binding free energies, ΔG_{fluor}, were calculated from the K_d values. In Table 1, the listed previously published K_d values are examples of the discrepancies that result from different experimental conditions and techniques. However, the values from footnote d of Table 1 were obtained under identical conditions using surface plasmon resonance (SPR) spectroscopy[39] and correlate well with the fluorescence data reported here. Both sets of data support a relative binding order of paromomycin, gentamicin C, neamine, G418, and ribostamycin, as did the binding isotherms. However, as a result of the tobramycin family of aminoglycosides not behaving in the fluorescence assay, a relative order of binding for all the desired aminoglycosides is not feasible on the basis of the fluorescence data alone.

Thermal Denaturation. To bypass the tobramycin family's problematic behavior, thermal denaturation was implemented to acquire the general sequence in binding affinity of the tobramycin family aminoglycosides to the A-site with respect

Table 1. K_d and ΔG_{bind} Values Obtained from Fluorescence Assay and K_d Values from Previously Published Data

antibiotic	charge	ΔG_{fluor} (kJ/mol)	K_d (μM)	literature K_d (μM)
neomycin	6			0.053,[c] 0.019,[d] 0.004[e]
paromomycin	5	−36.7	0.39	1.65,[c] 0.2,[d] 0.027[e]
ribostamycin	4	−27.8	16.35	16,[a] 25,[d] 2.38[e]
neamine	4	−29.4	7.39	10,[b] 7.8[d]
gentamicin C	4	−30.2	5.53	1.7[d]
G418 (Geneticin)	4	−27.8	14.52	

[a] Reference 36: Griffey, R. H.; Hofstadler, S. A.; Sannes-Lowery, K. A.; Ecker, D. J.; Crooke, S. T. *Proc. Natl. Acad Sci. U.S.A.* **1999**, *96*, 10129−10133. [b] Reference 37: Sucheck, S. J.; Wong, A. L.; Koeller, K. M.; Boehr, D. D.; Draker, K.; Sears, P.; Wright, G. D.; Wong, C.-H. *J. Am. Chem. Soc.* **2000**, *122*, 5230−5231. [c] Reference 38: Ryu, D. H.; Rando, R. R. *Bioorg. Med. Chem.* **2001**, *9*, 2601−2608. [d] Reference 39: Wong, C.; Hendrix, M.; Priestly, E. S.; Greenberg, W. A. *Chem. Biol.* **1998**, *5*, 397−406. [e] Reference 40: Pilch, D. S.; Kaul, M.; Barbieri, C. M.; Kerrigan, J. E. *Biopolymers* **2003**, *70*, 58−79.

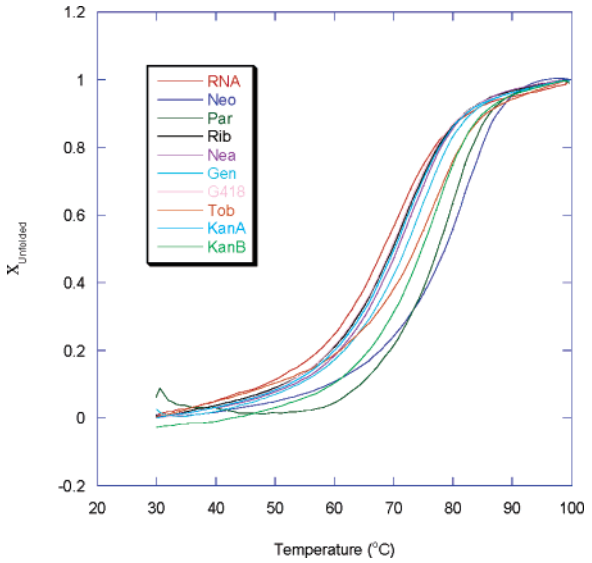

Figure 5. UV melting profile for A-site RNA and all of its aminoglycosides complexes at 100 mM ionic strength and pH 6.0.

Table 2. Thermal Stabilities and Free Energies from Fluorescence and Thermal Denaturation Experiments for Various Aminoglycosides

antibiotic	charge	T_m (°C)	ΔT_m (°C)	ΔG_{fluor} (kJ/mol)[a]	ΔG_{T_m} (kJ/mol)
A-site RNA		70.7			
neomycin	6	82.9	12.2	−44.20	−36.42
paromomycin	5	79.4	8.7	−36.70	−34.56
kanamycin B	5	77.5	6.8	−33.63	−33.53
tobramycin	5	76.0	5.3	−31.54	−32.71
gentamicin C	4	75.0	4.3	−30.20	−32.16
neamine	4	73.5	2.8	−29.40	−31.33
G418 (Geneticin)	4	72.4	1.7	−28.08	−30.72
kanamycin A	4	72.4	1.7	−27.80	−30.72
ribostamycin	4	72.0	1.3	−27.80	−30.50

[a] Italicized values were obtained via the second-order polynomial fit (ΔG_{exp} values).

to all of other aminoglycosides in this investigation. Melting curves were obtained for the A-site oligonucleotide in the absence and presence of neomycin, paromomycin, ribostamycin, neamine, tobramycin, kanamycin A, kanamycin B, gentamicin C, and G418 at an RNA−aminoglycoside ratio of 1:1 at a pH of 6.0 and an ionic strength of 100 mM (Figure 5). The thermal denaturation of the RNA−drug complex was performed twice for each aminoglycoside, and the mean of the two T_m values was calculated (Table 2). The presence of each aminoglycoside increased the thermal stability of the A-site duplex.

Although it has been suggested that a more distinct separation in T_m values, thus a more defined relative hierarchy, can be obtained at lower Na^+ concentrations, i.e., 60 mM,[29] an ionic strength of 100 mM ($[Na^+] = 95$ mM) was selected to avoid too much deviation from the value used in the fluorescence assay. The ΔT_m values for the neomycin, paromomycin, and ribostamycin−RNA complexes at $[Na^+] = 60$ mM were 12.0, 9.7, and 2.7 °C, respectively.[29] As shown in Table 2, neomycin, the strongest binder to the A-site RNA, increases the T_m of the A-site oligonucleotide by 12.2 °C and ribostamycin, the weakest binder, enhances duplex stability by 1.3 °C, which yields a larger range than the one afforded by the experiment conducted at $[Na^+] = 60$ mM. The extent of thermal stabilization afforded to the RNA by neomycin is almost identical for both the 60 and 95 mM concentration of Na^+ ions. However, the ΔT_m for paromomycin in the 60 mM Na^+ solution is 1 °C higher than the one for the 95 mM Na^+ solution. The variance in ribostamycin ΔT_m values for the different concentrations of Na^+ ions is even greater; the ΔT_m of the RNA−ribostamycin complex for the 60 mM Na^+ solution is 1.4 °C greater than for the one taken at 95 mM Na^+ solution. The trend is not surprising because lower Na^+ concentration means there is less entropy of stabilization due to counterion release as the aminoglycoside binds. Also, the difference in ΔT_m values ($\Delta\Delta T_m$) between the 60 and 95 mM Na^+ solutions increases as the affinity of the drug for the RNA decreases.

The T_m value for each of the aminoglycosides was used to calculate the transition free energy, ΔG_{T_m}, for each antibiotic using the equation $\Delta G = -RT \ln K_a$ where $T = 298$ K (Table 2). For these experiments, the free base forms of the aminoglycosides were used to remove the possibility of the sulfate ions influencing the thermal stability of the RNA−drug complexes. The sulfate ions from the aminoglycoside sulfate salts can thermally destabilize the complex by giving the positively charged aminoglycoside an alternative negatively charged target, especially when the concentrations of RNA and SO_4^{2-} are comparable. With strong A-site binders, such as neomycin and paromomycin, the sulfate ions should not detract from the stability of the RNA−drug complex. However, with the weaker binders, such as ribostamycin, the sulfate ions have the ability to interfere with the stability of the RNA−drug complex. So theoretically, if the T_m values had been obtained at $[Na^+] = 60$ mM using the free base forms of the aminoglycosides, the observed range of ΔT_m values would have been larger than those for the sulfate salts.

The extent of aminoglycoside-induced enhancement in RNA thermal stability follows the hierarchy neomycin > paromomycin > kanamycin B > tobramycin > gentamicin C > neamine > G418 > kanamycin A > ribostamycin. The order of the aminoglycoside binding affinities is in agreement with the fluorescence data, as shown in Table 2. The correlation between the free energies obtained from the fluorescence and thermal denaturation studies indicates that the order of affinity resulting from these experiments is very reliable.

It must be kept in mind that the free energies resulting from the thermal denaturation studies are not binding free energies. The ΔG_{T_m} represent the following events:

$$\begin{array}{ccc} \text{folded RNA} \bullet \text{AG} & \rightarrow & \text{unfolded RNA} \bullet \text{AG} \\ \downarrow & & \downarrow \\ \text{folded RNA} + \text{AG} & \rightarrow & \text{unfolded RNA} + \text{AG} \end{array}$$

The complex can undergo two different paths to arrive at the denatured, unbound state. The folded RNA can denature prior to separating from the aminoglycoside (AG) or separate itself

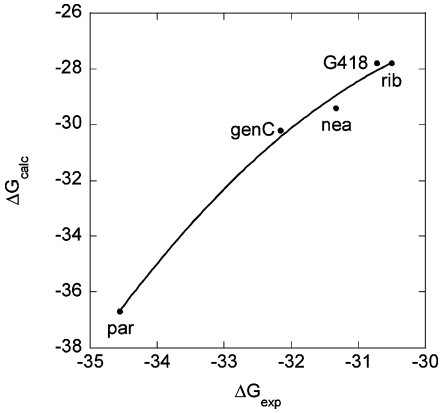

Figure 6. Plot of ΔG_{calc} vs ΔG_{exp} fit to a second-order polynomial.

from the AG first, then unfold. Obviously, these paths are not exclusive of each other; the actual path the complex takes to arrive at the denatured, unbound state is most likely a combination of the two explicit paths. Because of the unclear mechanism of denaturation, the ΔG_{T_m} values only indicate the extent of stabilization each aminoglycoside imparts upon the A-site oligonucleotide with respect to the unbound, folded A-site RNA. From the thermal stabilization data, the relative order of binding affinities can be inferred by assuming that a direct relationship exists between the two.

Interestingly, although the ΔG_{T_m} values do not describe a defined process, they do comprise a binding hierarchy that agrees very well with the data obtained from the fluorescence binding assay. Since there appears to be such a good correlation between the fluorescence and T_m data, a plot of ΔG_{fluor} versus ΔG_{T_m} for the neomycin and gentamicin family was generated to see if there was a quantitative relationship between the free energies obtained by the two different techniques. The data were plotted and fitted by a second-order polynomial ($y = (-215$ kJ$) - (13.5$ kJ$)x - (0.24$ kJ$)x^2$) to obtain a relationship with a R^2 value of 0.998. As shown by Figure 6, the fit is rather accurate, so this second-order polynomial was used to derive ΔG_{fluor} values for the aminoglycosides that did not behave well in the fluorescence assay. The values for ΔG_{fluor} will be the experimental values used to fit the parameters present in the theoretical binding free energy formula (ΔG_{calc} of eq 1). The free energies obtained from this second-order polynomial relationship and the ΔG_{fluor} values will be referred to as ΔG_{exp}. ΔG_{exp} values were extrapolated for neomycin, kanamycin B, tobramycin, and kanamycin A (Table 2). From this point on, the fluorescence free energies and the extrapolated free energies will be collectively referred to as ΔG_{exp}.

Computation for A-Site Oligonucleotide. Prior to APBS calculations on the entire 30S system with different aminoglycosides, APBS was tested on smaller, analogous A-site systems. The oligonucleotides used in all three crystal structures have the same core (Westhof construct), as shown in Figure 1c. The only difference between the RNAs is the 5′ overhang. The oligonucleotide used for the crystal structures 1J7T and 1MWL has a 5′ overhang of a single cytosine, while the 1LC4 structure contains RNA with a 5′ overhang of two uracils. The Westhof crystal structures were selected for the binding free energy calculations because the oligonucleotides used in these structures are nearly identical and the bound aminoglycosides have different core configurations, making them versatile. ΔG_{elec} values were calculated by solving the LPBE and NPBE for the following A-site/aminoglycoside complexes: (1J7T) neomycin, paromomycin, ribostamycin, and neamine; (1LC4), tobramycin, kanamycin A, and kanamycin B; (1MWL), G418 (Geneticin), and gentamicin C (components of gentamicin are gentamicin C2, gentamicin C1, and gentamicin C1a).

To obtain the ΔG_{elec} and ΔSASA values for gentamicin C, the contributions of all its components were calculated individually and then averaged. The ΔG_{elec} values are highly negative, reflecting the favorable electrostatic interactions between the charged aminoglycosidic rings and RNA (Table 3). The ΔG_{elec} values obtained from the solution of the LPBE are more favorable than those obtained from the NPBE (Table 3). Even though the LPBE is an approximation to NPBE, for a fixed dielectric both give similar order of binding showing the usefulness of both NPBE and LPBE for studying relative binding free energies. A dielectric of 4 assigned to the solute interior results in the paromomycin complex yielding a ΔG_{elec} value with a slightly greater magnitude than neomycin, which is contrary to experimental binding free energies. When the calculations are performed with a solute dielectric of 12, the ordering based on the electrostatic contributions within the family of aminoglycosides corresponds to the published experimental data quite well, suggesting better performance of higher dielectric for this system. Dielectric values above 10 were also previously suggested for proteins by other authors.[56−59]

The results from the APBS calculations for gentamicin C1a, C1, and C2 are nearly identical. This is not surprising because the differences between the chemical structures are minimal; they consist of whether a methyl group or a hydrogen atom occupies the R positions (Figure 2). However, the PB model in the APBS application is able to differentiate between ribostamycin and neamine and between tobramycin and kanamycin B even though the maximum number of charges is identical and their structures are similar. The difference between ribostamycin and neamine is that neamine lacks the D-ribose moiety (ring III). The difference in ΔSASA is expected because of the difference in size. However, although their protonation states are assumed to be the same, the ΔG_{elec} values for ribostamycin are consistently smaller than the ones for neamine. The 2′-NH_2 of tobramycin is more basic than kanamycin B,[31] but upon binding, their binding induced protonation states should be identical. Their structure differs only in that tobramycin has a hydrogen atom occupying the R2 position, whereas kanamycin B has a hydroxyl group (Figure 2). The hydroxyl group lends kanamycin B the ability to form an additional hydrogen bond to the RNA than tobramycin; thus, the ΔG_{elec} values for kanamycin B are larger than the ones for tobramycin, both computationally and experimentally. These values demonstrate that the PB implicit solvent model is sensitive enough to analyze the charge distribution and atomic interactions of the system in order to differentiate between the two compounds.

The computational values were fit to the experimental ΔG_{fluor} and extrapolated ΔG_{exp} values to obtain ΔG_{calc}. The translational and rotational entropy loss upon binding was assumed to be similar for every aminoglycoside and based on the reference[29] was set to 62.8 kJ/mol. The best physical sets of parameters for each dielectric constant for the LPBE- and NPBE-based calculations are listed in Table 4. Table 4 also lists the ΔG_{calc} values resulting from the parameters. The antibiotics are listed from the strongest to the weakest A-site binder, in accordance with the experimental data. The fitted γ values for the dielectric of 12 were larger than for the value of 4 and in the range of values used in the literature, which are from 21 [60] to 105 [61] to 250 J mol^{-1} Å^{-1}.[33,41] These suggest that γ is a parameter that has to be estimated for each system individually depending on the applied force field, dielectric constant, dielectric boundary

Table 3. Electrostatic Contribution (ΔG_{elec}) to Binding of Various Aminoglycosides and the Change in SASA upon Complexation with A-Site

			ΔG_{elec} (kJ/mol)				
			LPBE		NPBE		
antibiotic	charge	no. of rings	$\epsilon = 4$	$\epsilon = 12$	$\epsilon = 4$	$\epsilon = 12$	ΔSASA (Å^2)
1J7T							
neomycin	6	4	−182.7	−153.3	−135.7	−113.8	−1110
paromomycin	5	4	−186.4	−142.6	−144.4	−107.4	−1102
ribostamycin	4	3	−136.5	−109.7	−101.8	−80.9	−840
neamine	4	2	−148.5	−113.5	−114.9	−85.8	−668
1LC4							
tobramycin	5	3	−121.6	−116.2	−87.6	−87.7	−965
kanamycin A	4	3	−101.1	−95.1	−72.8	−71.2	−964
kanamycin B	5	3	−126.5	−118.1	−92.5	−89.7	−970
1MWL							
G418 (Geneticin)	4	3	−159.1	−116.6	−128.4	−90.4	−1002
gentamicin C1	5	3	−144.5	−122.7	−108.7	−92.0	−1030
gentamicin C1a	5	3	−141.3	−121.9	−105.3	−91.0	−969
gentamicin C2	5	3	−143.8	−122.9	−107.9	−92.1	−998
gentamicin C	5	3	−143.2	−122.5	−107.3	−91.7	−999

Table 4. ΔG_{calc} for All Aminoglycosides and the Best Fit Values for γ, Entropy Loss per Ring, and Additional Reorganizational Energy Determined from Calculated Values of ΔG_{elec}, ΔSASA, and $T\Delta S_{Tr+Rot}$ Values Estimated from Literature and ΔG_{exp}

	LPBE		NPBE	
parameter	$\epsilon = 4$	$\epsilon = 12$	$\epsilon = 4$	$\epsilon = 12$
γ (kJ mol^{-1} Å^{-2})	0.021	0.042	0.021	0.054
$T\Delta S_{conf}$ per ring (kJ mol^{-1})	23.7	16	NA	NA
$T\Delta S_{conf}$ per aminoglycoside (kJ mol^{-1})	NA	NA	34.65[a]	15.6[a]
ΔG_{strain} (kJ mol^{-1})	−3.7	4	NA	NA

aminoglycoside	ΔG_{calc} (kJ mol^{-1})			
neomycin	−52.0	−68.9	−61.5	−41.3
paromomycin	−55.6	−57.9	−70.1	−34.8
kanamycin B	−16.7	−44.0	−15.5	−27.3
tobramycin	−11.6	−41.8	−10.4	−25.1
gentamicin[b]	−33.9	−49.5	−31.4	−29.9
neamine	−55.9	−42.7	−31.4	−29.9
kanamycin A	9.4	−20.5	4.4	−8.6
G418	−49.9	−43.7	−52.0	−28.5
ribostamycin	−23.9	−30.0	−22.0	−15.7

[a] This value includes the entropy loss for the entire aminoglycoside (similar for every studied antibiotic), not for each individual ring together with the ΔG_{strain} energy. To obtain an estimate of the entropy loss per ring for a specific aminoglycoside, this value has to be divided by the number of rings it is composed of. [b] The ΔG_{calc} values for gentamicin are the averages of gentamicin C1, C1a, and C2.

definition, and type of solute. Also, the model used by us for the nonpolar term includes both hydrophobic contributions and van der Waals interactions between the antibiotic and RNA. Another approach exists that includes hydrophobic contributions in the SASA term, but the van der Waals interactions are calculated explicitly.[62] These models result in different microscopic surface tensions. The $T\Delta S_{conf}$ best fit term represents the fitted entropy loss per ring or per the entire aminoglycoside. The $T\Delta S_{conf}$ values per ring obtained for the LPBE with a dielectric of 4 are larger when compared to the scale developed by Pickett and Sternberg (1993).[63] Pickett and Sternberg's values for the main chain and side chain entropy loss of the protein residue upon folding are around 12 kJ/mol, so the fitted $T\Delta S_{conf}$ values obtained for the LPBE with a dielectric of 12 and the NPBE with a dielectric of 4 are most similar to published values. However, one has to bear in mind that the Pickett and Sternberg values were estimated for proteins and may be taken only as a rough measure of the entropy loss in the case of other systems. For both the LPBE- and NPBE-based calculations, a dielectric of 12 results in the best set of parameters. As shown in Table 4, neither solute dielectric of 4 or 12 for both the LPBE and NPBE calculations maintains an overall relative order of binding identical to the one obtained from the experimental data. However, with a dielectric of 12, the hierarchy of binding affinities correlates with experimental data within the family of aminoglycosides. This aspect can be exploited to determine relative binding affinities of modified aminoglycosides to their parent compounds.

The order of relative binding is maintained within each family of aminoglycosides for both the LPBE- and NPBE-based calculations with a solute dielectric constant of 12. The LPBE-based calculations yield more negative ΔG_{calc} values and a larger range of ΔG_{calc} values than the NPBE-based calculations, resulting in a more pronounced difference in the relative binding free energies.

For the dielectric of 12, ΔG_{calc} was plotted against ΔG_{exp} and subjected to a linear curve fit, resulting in R^2 values (Figures 7 and 8). The R^2 values were used to determine the extent of correlation between the calculated and experimental binding free energies. With both LPBE and NPBE derived ΔG_{calc}, when all of the aminoglycosides are plotted, the R^2 values were 0.710 and 0.622, respectively, which is indicative of a moderately good fit, with the fit for the LPBE being slightly better than that for the NPBE. However, when the different families of aminoglycosides were plotted individually, the R^2 factors were greater than 0.9, indicating a good correlation between the aminoglycosides within the family. It appears that both the LPBE- and NPBE-based APBS calculations are applicable to the A-site system when the dielectric constant is set to 12 and each aminoglycoside family is analyzed independently, as postulated in previous studies.[56−58] In theory, the NPBE-based calculations should be better, but it seems that the LPBE yields good results as well, as demonstrated by the respective R^2 values.

Computations for the Entire 30S Complex. The electrostatic contributions of the neomycin family aminoglycosides and streptomycin were calculated on the basis of modified versions of 1FJG crystal structure.[49] This structure was selected because of its versatility and the best available resolution. It has three aminoglycosides with different core structures bound to the 30S subunit, so all three aminoglycosides can be used as the basis for other modified aminoglycosides. APBS calculations were performed for streptomycin to determine if the parameters obtained for the A-site/2-DOS system can be extended to the antibiotic that does not share the 2-DOS core, has a relatively small charge, and is not specific to the A-site. Also, there is a previously published experimental K_d available for streptomycin to the A-site oligonucleotide,[39] so the calculated 30S data were

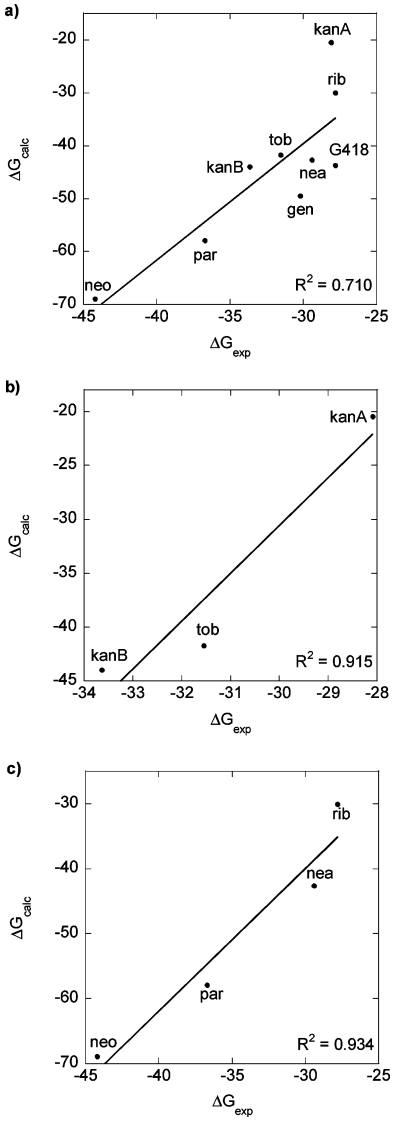

Figure 7. ΔG_{calc} ($\epsilon = 12$) generated from the solution of the LPBE vs ΔG_{exp} plot for (a) all the aminoglycosides, (b) the tobramycin family, and (c) the neomycin family.

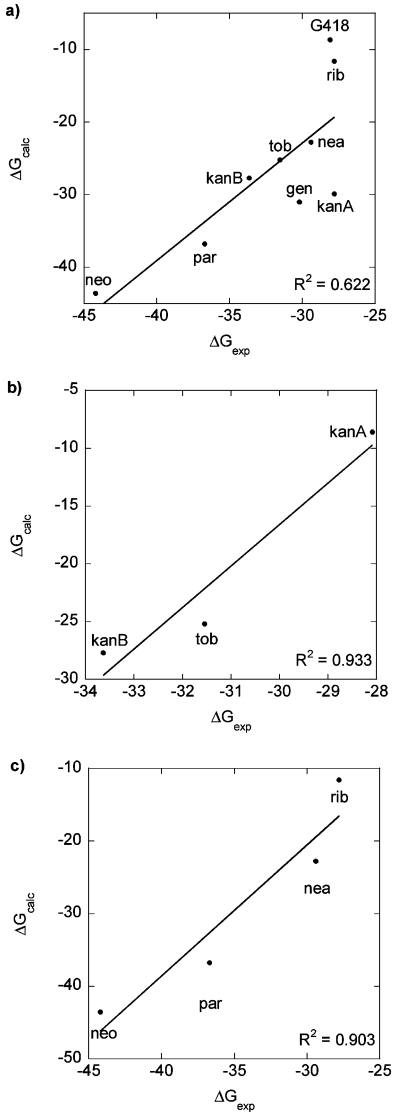

Figure 8. Obtained from the solution of the NPBE ($\epsilon = 12$) ΔG_{calc} vs ΔG_{exp} plot for (a) all the aminoglycosides, (b) the tobramycin family, and (c) the neomycin family.

Table 5. 30S Complex ΔG_{elec} Values Obtained from the Solution of the LPBE for Dielectric Constants of 4 and 12 and ΔSASA Values

		ΔG_{elec} (kJ/mol)		
aminoglycoside	charge	$\epsilon = 4$	$\epsilon = 12$	ΔSASA (Å^2)
neomycin	6	−328	−296	−1091
paromomycin	5	−298	−262	−1077
ribostamycin	4	−153	−155	−821
neamine	4	−177	−172	−641
streptomycin	2	−48	−75	−956

directly fit to the A-site experimental data to see if a good fit can be obtained by relating the K_d from a subsystem to binding free energy of the larger one.

For the 30S subunit, only the LPBE-based APBS calculations were performed (see Materials and Methods). However, previous calculations on the A-site fragment demonstrated that the LPBE results in the correct binding hierarchy within a family of aminoglycosides. Moreover, a previous APBS study for the antibiotics binding to the 30S subunit showed that LPBE is a reliable approximation for analyzing the relative binding free energies even though this study used a less detailed model for estimating the binding free energies incorporating only the electrostatic and nonpolar contributions.[50] The set of aminoglycosides that were studied did not include the tobramycin and gentamycin families.

Table 6. Parameters for the 30S Subunit That Were Fitted on the Basis of ΔG_{elec} and SASA Values Using the A-Site ΔG_{exp} for the Neomycin Family[a]

parameter	$\epsilon = 4$	$\epsilon = 12$
γ (kJ mol^{-1} Å^{-2})	0.2	0.021
$T\Delta S_{conf}$ per ring (kJ mol^{-1})	117	30
ΔG_{strain} (kJ mol^{-1})	−50	10

		no.	ΔG_{calc} (kJ mol^{-1})		ΔG_{exp}
aminoglycoside	charge	rings	$\epsilon = 4$	$\epsilon = 12$	(kJ mol^{-1})
neomycin	6	4	−65.1	−126.4	−44.2
paromomycin	5	4	−33.0	−91.3	−36.7
neamine	4	3	−58.0	−52.7	−27.8
ribostamycin	4	2	46.3	−9.3	−29.4
streptomycin	2	3	124.6	67.8	−23.0

[a] ΔG_{calc} for streptomycin was obtained by using the listed parameters.

Table 5 lists the results for the APBS calculations for the 30S subunit and the following aminoglycosides: neomycin, paromomycin, neamine, ribostamycin, and streptomycin. The ΔG_{elec} correlates well with the binding hierarchy established by the experimental results. Streptomycin was not a part of the

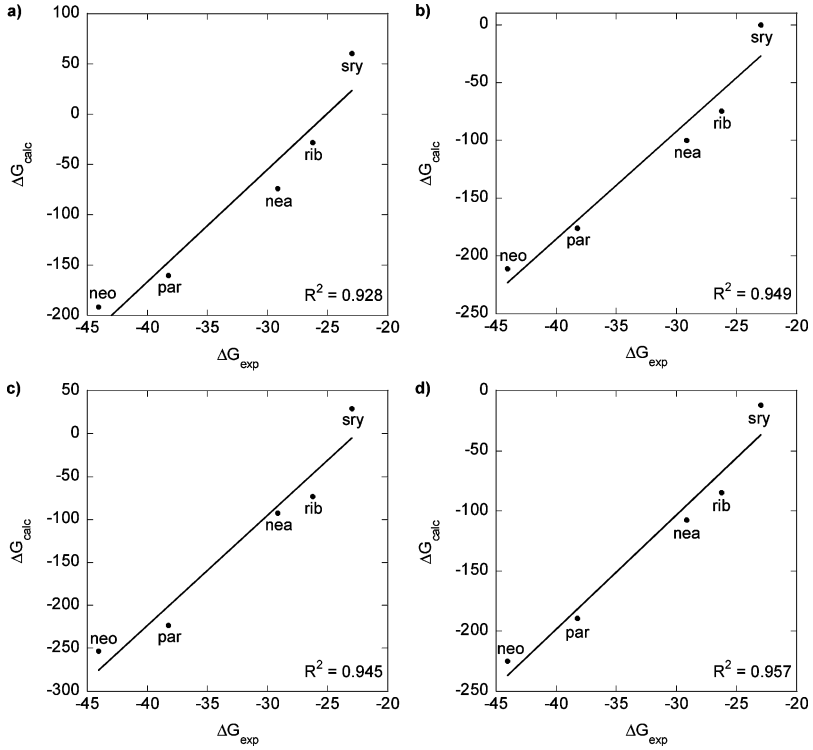

Figure 9. Plot of relative ΔG_{calc} against ΔG_{exp} for the LPBE-based calculations for the 30S subunit and parameters obtained from the fit for the LPBE-based A-site oligonucleotide calculations (see Table 4) (a) with a dielectric of 4 and $\gamma = 0.021$ kJ mol^{-1} Å^{-1}, $T\Delta S_{conf}$ per ring = 23.7 kJ mol^{-1}, $\Delta G_{strain} = -3.7$ kJ mol^{-1} and (b) with a dielectric of 12 and $\gamma = 0.042$ kJ mol^{-1} Å^{-1}, $T\Delta S_{conf}$ per ring = 16 kJ mol^{-1}, $\Delta G_{strain} = 4$ kJ mol^{-1}. Plot of relative ΔG_{calc} against ΔG_{exp} for the LPBE-based calculations for the 30S subunit and parameters obtained from the fit for the NPBE-based A-site oligonucleotide calculations (c) with a dielectric of 4 and $\gamma = 0.021$ kJ mol^{-1} Å^{-1}, $T\Delta S_{conf}$ per aminoglycoside = 34.7 kJ mol^{-1} and (d) with a dielectric of 12 and $\gamma = 0.054$ kJ mol^{-1} Å^{-1}, $T\Delta S_{conf}$ per aminoglycoside = 15.6 kJ mol^{-1}.

experimental work done in this study, but its K_d of 95 μM has been previously published.[64] According to the order dictated by the ΔG_{elec} values and its K_d and charge, streptomycin is in a reasonable position in the hierarchy of binding. The two dielectric constants yield similar ΔG_{elec} for all the aminoglycosides except streptomycin. The ΔG_{elec} value for streptomycin is $^2/_3$ greater when the dielectric is set to 12 rather than 4. The ΔSASA corresponds well to the number of rings comprising each aminoglycoside.

The calculated values for the neomycin family of aminoglycosides were subjected to a least-squares fit to experimental values for the A-site oligonucleotide because of the dearth of experimental values for the entire 30S subunit. Streptomycin was not fit to its published value because it was obtained by a different experimental method. Table 6 lists the parameters and ΔG_{calc} values for this fit. ΔG_{calc} for streptomycin was obtained by using the parameters obtained by the neomycin family fit. Both of the dielectric constants yield ΔG_{calc} values that coincide with the aminoglycosides' affinity to A-site RNA. These parameters give positive values for the ΔG_{calc} of streptomycin, but the relative order of binding is maintained.

The parameters that were obtained for the A-site calculations under various conditions were used to obtain ΔG_{calc} values and to determine their applicability to the 30S subunit (Figure 9). The relative order of binding was maintained throughout the various sets of parameters; however, the ΔG_{calc} values for a dielectric constant of 4 were not as favorable as the ones for the dielectric of 12. For streptomycin, when $\epsilon = 4$, the ΔG_{calc} values were positive, whereas for the dielectric constant of 12, the resulting ΔG_{calc} values were negative, thus demonstrating that a dielectric constant of 12 is better suited for the 30S system when applying the fitted parameters from the A-site calculations.

ΔG_{calc} was plotted against ΔG_{exp} to obtain the R^2 factor and determine the extent of correlation between the two free energy values (Figures 9). All four sets of data resulted in good correlation between the experimental and the computational data; however, the dielectric of 12 results again in the best R^2 values. Including streptomycin into the plot (ΔG_{SPR} value for streptomycin was used as ΔG_{exp}) caused the R^2 factors for the dielectric constant of 12 to decrease slightly. On the other hand, the correlation of the experimental to computational data increases slightly upon inclusion of streptomycin for the dielectric constant of 4. Overall, it appears that a dielectric of 12 and the LPBE are more amenable to the 30S subunit, although the distinction between the LPBE- and NPBE-derived A-site parameters applied to the 30S system is small.

Conclusions

We studied the binding of aminoglycosides to the A-site model and to the 30S small ribosomal subunit by Poisson−Boltzmann implicit solvent methodology. To be able to compare the computational results with the experimental data under similar conditions, we performed thermal denaturation studies and fluorescence binding assay.

The limitations of the computational studies for the whole 30S subunit that result in the electrostatic contribution of the binding free energy must be borne in mind. These include single conformation approximation for the complex and associating molecules, the choice of parameters such as partial charges, van der Waals radii, molecular surface definition, and the quality of the crystal structure. Despite those limitations, the PB implicit solvent model in the APBS application appears to be a relatively quick and reliable method to obtain relative orders of binding to the A-site and the 30S subunit even though the absolute

binding free energies are not always in accord with experimental ones, especially for the 30S subunit. The LPBE approximation seems sufficient and more amenable to the A-site and the 30S subunit, although both the NPBE and LPBE resulted in the correct binding hierarchy. The implicit solvent PB method has the ability to perceive small charge perturbations caused by different functional groups. In cases where the electrostatics dominates binding and changes in the studied ligand structure result in changes of its net charge, the implicit solvent Poisson−Boltzmann model works well. In cases where there are very subtle changes however, such as changing a hydrogen into a methyl group, the effect cannot be predicted. As the computational data show, for the A-site system, the aminoglycosides adhered to the binding hierarchy within the family, and for the 30S system, it appears that such calculations can be extended to aminoglycosides lacking the 2-DOS ring. The preference for the A-site and 30S system for the dielectric of 12 indicates that in both systems the potential seems to be more capable of changing with their immediate environment, thus allowing the accommodation of many different electrostatically driven interactions. This could explain the ability of the A-site to complex to various types of ligands, making the A-site and the 30S subunit a good drug target.

Overall, despite many approximations, the implicit solvent PB approach and the APBS and the binding energy calculation protocol applied in this study are amenable to investigation of the binding hierarchy of aminoglycosides to the A-site and 30S. The method would be a useful tool in drug-discovery environments where estimations and speed are crucial to determining which modified aminoglycosides present the greatest probability of increased binding to the A-site.

Acknowledgment. We thank Dr. Charles Liu for his generous donation of neamine and Dr. Kenneth Blount for his helpful discussion. This work was supported in part by NIH, NSF, the Howard Hughes Medical Institute, the National Biomedical Computational Resource, the NSF Center for Theoretical Biological Physics, the W. M. Keck Foundation, and Accelrys Inc. J.T. was supported by the Polish Ministry of Science (Grant 3T11F 005 30) and Warsaw University (Grants 115/E-343/ICM/BST-1076/2005 and 115/30/E-343/S/BST-1140/ICM/2006).

References

(1) Walter, F.; Vincens, Q.; Westhof, E. Aminoglycoside−RNA interactions. *Curr. Opin. Chem. Biol.* **1999**, *3*, 694−704.
(2) Cashman, D. J.; Rife, J. P.; Kellogg, G. E. Which aminoglycoside ring is most important for binding? A hydropathic analysis of gentamicin, paromomycin and analogues. *Bioorg. Med. Chem. Lett.* **2001**, *11*, 119−122.
(3) Davies, J.; Gorini, L.; Davis, B. D. Misreading of RNA codewords induced by aminoglycoside antibiotics. *Mol. Pharmacol.* **1965**, *1*, 93−106.
(4) Moazed, D.; Noller, H. F. Interaction of antibiotics with functional sites in 16S ribosomal RNA. *Nature* **1987**, *327*, 389−394.
(5) Karimi, R.; Ehrenberg, M. Dissociation rate of cognate peptidyl tRNA from the A-site of hyper-accurate and error-prone ribosomes. *Eur. J. Biochem.* **1994**, *226*, 355−360.
(6) Yoshizawa, S.; Fourmy, D.; Puglisi, J. D. Recognition of the codon−anticodon helix by ribosomal RNA. *Science* **1999**, *285*, 1722−1725.
(7) Pape, T.; Wintermeyer, W.; Rodnina, M. V. Conformational switch in the decoding region of the 16S rRNA during aminoacyl−tRNA selection on the ribosome. *Nat. Struct. Biol.* **2000**, *7*, 104−107.
(8) Carter, A. P.; Clemons, W. M.; Brodersen, D. E.; Morgan-Warren, R. J.; Wimberly, B. T.; Ramakrishnan, V. Functional insights from the structure of the 30S ribosomal subunit and its interactions with antibiotics. *Nature* **2000**, *407*, 340−348.
(9) Vicens, Q.; Westhof, E. RNA as a drug target: the case of aminoglycosides. *ChemBioChem.* **2003**, *4*, 1018−1023.
(10) Yusupov, M. M.; Yusupova, G. Z.; Baucom, A.; Lieberman, K.; Earnest, T. N.; Cate, J. H. D.; Noller, H. F. Crystal structure of the ribosome at 5.5 Å resolution. *Science* **2000**, *292*, 883−896.
(11) Ogle, J. M.; Brodersen, D. E.; Clemons, W. M.; Tarry, M. J.; Carter, A. P.; Ramakrishnan, V. Recognition of cognate transfer RNA by the 30S ribosomal subunit. *Science* **2001**, *292*, 897−902.
(12) Carter, A. P.; Clemons, W. M.; Brodersen, D. E.; Morgan-Warren, R. J.; Hartsch, T.; Wimberly, B. T.; Ramakrishnan, V. Crystal structure of an initiation factor bound to the 30S ribosomal subunit. *Science* **2001**, *291*, 498−501.
(13) Brodersen, D. E.; Clemons, W. M.; Carter, A. P.; Morgan-Warren, R. J.; Wimberly, B. T.; Ramakrishnan, V. The structural basis for the action of the antibiotics tetracycline, pactamycin, and hygromycin B on the 30S ribosomal subunit. *Cell* **2000**, *103*, 1143−1154.
(14) Pfister, P.; Hobbie, S.; Vicens, Q.; Bottger, E. C.; Westhof, E. The molecular basis for A-site mutations conferring aminoglycoside resistance: Relationship between ribosomal susceptibility and X-ray crystal structures. *ChemBioChem.* **2003**, *4*, 1078−1088.
(15) Lynch, S. R.; Gonzalez, R. L.; Puglisi, J. D. Comparison of X-ray crystal structure of the 30S subunit−antibiotic complex with NMR structure of decoding site oligonucleotide−paromomycin complex. *Structure* **2003**, *11*, 43−53.
(16) Shandrick, S.; Zhao, Q.; Han, Q.; Ayida, B. K.; Takahashi, M.; Winters, G. C.; Simonsen, K. B.; Vourloumis, D.; Hermann, T. Monitoring molecular recognition of the ribosomal decoding site. *Angew. Chem., Int. Ed.* **2004**, *43*, 3177−3182.
(17) Kaul, M.; Barbieri, C. M.; Pilch, D. S. Fluorescence-based approach for detecting and characterizing antibiotic-induced conformational changes in ribosomal RNA: comparing aminoglycoside binding to prokaryotic and eukaryotic ribosomal RNA sequences. *J. Am. Chem. Soc.* **2003**, *126*, 3447−3453.
(18) Wimberly, B. T.; Brodersen, D. E.; Clemons, W. M.; Morgan-Warren, R. J.; Carter, A. P.; Vonrhein, C.; Hartsch, T.; Ramakrishnan, V. Structure of the 30S ribosomal unit. *Nature* **2000**, *407*, 327−339.
(19) Ogle, J. M.; Murphy, F. V.; Tarry, M. J.; Ramakrishnan, V. Selection of tRNA by the ribosome requires a transition from an open to a closed form. *Cell* **2002**, *111*, 721−732.
(20) Purohit, P.; Stern, S. Interactions of a small RNA with antibiotic and RNA ligands of the 30S subunit. *Nature* **1994**, *370*, 659−662.
(21) Recht, M. I.; Fourmy, D.; Blanchard, S. C.; Dahlquist, K. D.; Puglisi, J. D. RNA sequence determinants for aminoglycoside binding to an A-site rRNA model oligonucleotide. *J. Mol. Biol.* **1996**, *262*, 421−436.
(22) Recht, M.; Douthwaite, S.; Dahlquist, K. D.; Puglisi, J. D. Effect of mutations in the A site of 16 S rRNA on aminoglycoside antibiotic−ribosome interaction. *J. Mol. Biol.* **1999**, *286*, 33−43.
(23) Fourmy, D.; Recht, M. I.; Puglisi, J. D. Binding of neomycin-class aminoglycoside antibiotics to the A-site of 16S rRNA. *J. Mol. Biol.* **1998**, *277*, 347−362.
(24) Fourmy, D.; Recht, M. I.; Blanchard, S. C.; Puglisi, J. D. Structure of the A-site of *Escherichia coli* 16S ribosomal RNA complexed with an aminoglycoside antibiotic. *Science* **1996**, *274*, 1367−1371.
(25) Jean, J. M.; Hall, K. B. 2-Aminopurine electronic structure and fluorescence properties in DNA. *Biochemistry* **2002**, *41*, 13152−13161.
(26) Vicens, Q.; Westhof, E. Crystal structure of paromomycin docked into the eubacterial ribosomal decoding A-site. *Structure* **2001**, *9*, 647−658.
(27) Vicens, Q.; Westhof, E. Crystal structure of a complex between the aminoglyciside tobramycin and an oligonucleotide containing the ribosomal decoding A-site. *Chem. Biol.* **2002**, *9*, 747−755.
(28) Vicens, Q.; Westhof, E. Crystal structure of Geneticin bound to a bacterial 16S ribosomal RNA A-site oligonucleotide. *J. Mol. Biol.* **2003**, *326*, 1175−1188.
(29) Kaul, M.; Pilch, D. S. Thermodynamics of aminoglycoside−rRNA recognition: the binding of neomycin-class aminoglycosides to the A site of 16S rRNA. *Biochemistry* **2002**, *41*, 7695−7706.
(30) Barbieri, C. M.; Srinivasan, A. R.; Pilch, D. S. Deciphering the origins of observed heat capacity changes for aminoglycoside binding to prokaryotic and eukaryotic ribosomal RNA A-sites: a calorimetric, computational, and osmotic stress study. *J. Am. Chem. Soc.* **2004**, *126*, 14380−14388.
(31) Wang, H.; Tor, Y. Electrostatic interactions in RNA aminoglycosides binding. *J. Am. Chem. Soc.* **1997**, *119*, 8734−8735.
(32) Hermann, T.; Westhof, E. Docking of cationic antibiotics to negatively charged pockets in RNA folds. *J. Med. Chem.* **1999**, *42*, 1250−1261.
(33) Honig, B.; Nicholls, A. Classical electrostatics in biology and chemistry. *Science* **1995**, *268*, 1144−1149.
(34) Debye, P.; Huckel, E. Zur Theorie der elektrolyte. I. Gefrierpunktserniedrigung und verwandte erscheinungen (On the theory of electrolytes. I. Freezing point depression and related phenomena). *Phys. Z.* **1923**, *24*, 185.

(35) Davis, M. E.; McCammon, J. A. Electrostatics in biomolecular structure and dynamics. *Chem. Rev.* **1990**, *90*, 509−521.
(36) Griffey, R. H.; Hofstadler, S. A.; Sannes-Lowery, K. A.; Ecker, D. J.; Crooke, S. T. Determinants of aminoglycoside-binding specificity for rRNA by using mass spectrometry. *Proc. Natl. Acad. Sci. U.S.A.* **1999**, *96*, 10129−10133.
(37) Sucheck, S. J.; Wong, A. L.; Koeller, K. M.; Boehr, D. D.; Draker, K.; Sears, P.; Wright, G. D.; Wong, C.-H. Design of bifunctional antibiotics that target bacterial rRNA and inhibit resistance-causing enzymes. *J. Am. Chem. Soc.* **2000**, *122*, 5230−5231.
(38) Ryu, D.-H.; Rando, R. R. Aminoglycoside binding to human and bacterial A-site rRNA decoding region constructs. *Bioorg. Med. Chem.* **2001**, *9*, 2601−2608.
(39) Wong, C.-H.; Hendrix, M.; Priestley, E. S.; Greenberg, W. A. Specificity of aminoglycoside antibiotics for the A-site of the decoding region of ribosomal RNA. *Chem. Biol.* **1998**, *5*, 397−406.
(40) Pilch, D. S.; Kaul, M.; Barbieri, C. M.; Kerrigan, J. E. Thermodynamics of aminoglycoside−rRNA recognition. *Biopolymers* **2003**, *70*, 58−79.
(41) Froloff, N.; Windemuth, A.; Honig, B. On the calculation of binding free eneregies using continuum methods: application to MHC class I protein−peptide interactions. *Protein Sci.* **1997**, *6*, 1293−1301.
(42) Konecny, R.; Trylska, J.; Tama, F.; Zhang, D.; Baker, N. A.; Brooks, C. L.; McCammon, J. A. Electrostatic properties of cowpea chlorotic mottle virus and cucmber mosaic virus capsids. *Biopolymers* **2006**, *82*, 106−120.
(43) Baker, N. A.; Joseph, D. S.; Holst, M. J.; McCammon, J. A. Electrostatics of nanosystems: application to microtubules and the ribosome. *Proc. Natl. Acad. Sci. U.S.A.* **2001**, *98*, 10037−10041.
(44) Gilson, M. K.; Sharp, K. A.; Honig, B. Calculating the electrostatic potential of molecules in solution: method and error assessment. *J. Comput. Chem.* **1988**, *9*, 327−335.
(45) Cornell, W. D.; Cieplak, P.; Bayly, C. I.; Gould, I. R.; Merz, K. M. J.; Ferguson, D. M.; Spellmeyer, D. C.; Fox, T.; Caldwell, J. W.; Kollman, P. A. A second generation force field for the simulation of proteins, nucleic acids, and organic molecules. *J. Am. Chem. Soc.* **1995**, *117*, 5179−5197.
(46) *InsightII*, version 2000; Molecular Simulations: San Diego, CA, 2000.
(47) Jakalian, A.; Bush, B. L.; Jack, D. B.; Bayly, C. I. Fast, efficient generation of high quality atomic charges. AMC1-BCC model. I: Method. *J. Comput. Chem.* **2000**, *21*, 132−146.
(48) Brooks, B. R.; Broccoleri, R. E.; Olafson, B. D.; States, D. J.; Swaminathan, S.; Karplus, M. CHARMM: a program for macromolecular energy, minimization, and dynamics calculations. *J. Comput. Chem.* **1983**, *4*, 187−217.
(49) Berman, H. M.; Westbrook, J.; Feng, Z.; Gilliland, G.; Bhat, T. N.; Weissig, H.; Shindyalov, I. N.; Bourne, P. E. The Protein Data Bank. *Nucleic Acids Res.* **2000**, *28*, 235−242.
(50) Ma, C.; Baker, N. A.; Joseph, S.; McCammon, J. A. Binding of aminoglycoside antibiotics to the small ribosomal subunit: a continuum electrostatics investigation. *J. Am. Chem. Soc.* **2002**, *124*, 1438−1442.
(51) Trylska, J.; McCammon, J. A.; Brooks, C. L. Exploring the assembly of the 30S ribosomal subunit using an implicit solvent approach. *J. Am. Chem. Soc.* **2005**, *127*, 11125−11133.
(52) Fogolari, F.; Zuccato, P.; Esposito, G.; Viglino, P. Biomolecular electrostatics with the linearized Poisson−Boltzmann equation. *Biophys. J.* **1999**, *76*, 1−16.
(53) Umezawa, S.; Tatsuta, K.; Tsuchiya, T.; Kitazawa, E. Synthesis of neamine. *J. Antibiot. (Tokyo)* **1967**, *20*, 53−54.
(54) Umezawa, H.; Kondo, S. Ion-exchange chromatography of aminoglycoside antibiotics. *Methods Enzymol.* **1975**, *43*, 263−278.
(55) Michael, K.; Wang, H.; Tor, Y. Enhanced RNA binding of dimerized aminoglycosides. *Bioorg. Med. Chem.* **1999**, *7*, 1361−1371.
(56) Dominy, B.; Brooks, C. Development of a generalized Born model parametrization for proteins and nucleic caids. *J. Phys. Chem. B* **1999**, *103*, 3765−3773.
(57) Grycuk, T. Deficiency of the Coulomb-field approximation in the generalized Born model: An improved formula for Born radii approximation. *J. Chem. Phys.* **2003**, *119*, 4817−4826.
(58) Miyashita, O.; Onuchic, J. N.; Okamura, M. Y. Continuum electrostatic model for the binding of cytochrome *c2* to the photosynthetic reaction center form *Rhodobacter sphaeroides*. *Biochemistry* **2003**, *42*, 11651−11660.
(59) Antosiewicz, J.; McCammon, J. A.; Gilson, M. K. Prediction of pH-dependent properties of proteins. *J. Mol. Biol.* **1994**, *238*, 415−436.
(60) Sitkoff, D.; Sharp, K. A.; Honig, B. Accurate calculation of hydration free energies using macroscopic solvent models. *J. Phys. Chem.* **1994**, *98*, 1978−1988.
(61) Wong, C. F.; Hunenberger, P. H.; Akamine, P.; Narayana, N.; Diller, T.; McCammon, J. A.; Taylor, S.; Xuong, N. Computational analysis of PKA−balanol interactions. *J. Med. Chem.* **2001**, *44*, 1530−1539.
(62) Levy, R. M.; Zhang, L. Y.; Gallicchio, E.; Felts, A. K. On the nonpolar hydration free energy of proteins: Surface area and continuum solvent models for the solute−solvent interaction energy account. *J. Am. Chem. Soc.* **2003**, *125*, 9523−9530.
(63) Pickett, S. D.; Sternberg, M. J. E. Empirical scale of side-chain conformational entropy in protein folding. *J. Mol. Biol.* **1993**, *231*, 825−839.
(64) Alper, P. B.; Hendrix, M.; Sears, P.; Wong, C.-H. Probing the specificity of aminoglycoside−ribosomal RNA interactions with designed synthetic analogs. *J. Am. Chem. Soc.* **1998**, *120*, 1965−1978.

JM060288O